Received 24 September 2015; accepted 9 October 2015. Date of publication 12 October 2015; date of current version 18 December 2015.
The review of this paper was arranged by Editor S. Moshkalev.

Digital Object Identifier 10.1109/JEDS.2015.2490178

All-Graphene Planar Double-Quantum-Dot Resonant Tunneling Diodes

FERAS AL-DIRINI[1,2] (Student Member, IEEE), MAHMOOD A. MOHAMMED[3], FARUQUE M. HOSSAIN[1], THAS (AMPALAVANAPILLAI) NIRMALATHAS[4] (Senior Member, IEEE), AND EFSTRATIOS SKAFIDAS[1] (Senior Member, IEEE)

1 Department of Electrical and Electronic Engineering and the Centre for Neural Engineering, University of Melbourne, Parkville, VIC 3010, Australia
2 Victorian Research Laboratory, National ICT Australia, West Melbourne, VIC 3003, Australia
3 Department of Electrical Engineering, Princess Sumaya University of Technology, Amman 11941, Jordan
4 Department of Electrical and Electronic Engineering and the Melbourne Networked Society Institute, University of Melbourne, Parkville, VIC 3010, Australia

CORRESPONDING AUTHOR: F. AL-DIRINI (e-mail: alf@unimelb.edu.au)

ABSTRACT This paper proposes a new class of resonant tunneling diodes (RTDs) that are planar and realizable with a single graphene nanoribbon. Unlike conventional RTDs, which incorporate vertical quantum well regions, the proposed devices incorporate two confined planar quantum dots within the single graphene nanoribbon, giving rise to a pronounced negative differential resistance (NDR) effect. The proposed devices, termed here as planar double-quantum-dot RTDs, and their transport properties are investigated using quantum simulations based on nonequilibrium Green's function formalism and the extended Huckel method. The proposed devices exhibit a unique current–voltage waveform consisting of a single pronounced current peak with an extremely high, in the order of 10^4, peak-to-valley ratio. The position of the current peak can be tuned between discrete voltage levels, allowing digitized tunability, which is exploited to realize multi-peak NDR devices.

INDEX TERMS Graphene, negative differential resistance, NDR, planar, quantum dot, tunable, resonant tunneling.

I. INTRODUCTION

Graphene, due to its exceptional electronic properties [1], has become a popular candidate for next generation electronics [2]. However, its lack of an electronic bandgap stands as an obstacle towards realizing high performance graphene field effect devices [3]. Accordingly, much effort has been directed towards the realization of graphene tunneling devices [4]–[6], which are promising candidates for next-generation electronics [7]. Graphene tunneling devices can achieve very high on-off ratios [4], an essential property for efficient switching. However, their full potential lies in achieving resonant tunneling, which gives rise to a property known as Negative Differential Resistance (NDR) [8]. This property enables devices that can be used as ultra-fast logic and memory devices [9] as well as high frequency oscillators operating well into the Terahertz regime [10]–[12].

An essential component of any tunneling device is the barrier across which electrons tunnel. In graphene tunneling devices this barrier can be another 2D material such as hexagonal Boron Nitride (hBN) stacked on top of graphene [4], [13]. However, such an approach gives rise to a vertical device, which requires vertical stacking and precise alignment of multiple graphene layers [13]. Moreover, the introduction of multiple barriers within such a device, in order to realize a double barrier resonant tunneling diode (DB-RTDs) [14], requires further stacking and alignment of more graphene layers. In order to overcome such a drawback, an in-plane barrier was previously proposed, by incorporating an insulating trench in a graphene nanoribbon (GNR) along its transport direction [15], giving rise to a completely planar device architecture; an all-graphene planar DB-RTD [15]. An all-graphene planar DB-RTD is schematically shown in Fig. 1(a).

Double barrier RTDs are able to achieve enhanced NDR due to the presence of a quantum confinement region within them, the region defined by the double barriers,

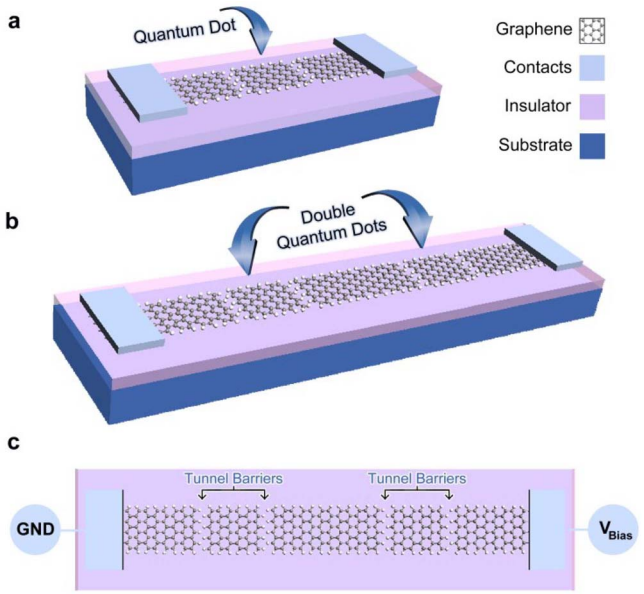

FIGURE 1. (a) 3D perspective views of the all-graphene planar double-barrier (single-quantum-dot) and (b) double-quantum-dot resonant tunneling diodes (RTDs), highlighting the positions of the quantum dots. (c) Top view of the device in (b) showing the bias direction and highlighting the position of the tunnel barriers.

in which electrons resonate. In conventional vertical DB-RTDs [10]–[12], [14], this is referred to as a quantum well, and is usually a thin semiconductor layer sandwiched vertically between two layers of another material with a larger bandgap. In the all-graphene planar DB-RTDs [15], the quantum well region is replaced by a length of the GNR that is isolated by the in-plane insulating trenches, forming a more confined structure; a zero-dimensional graphene quantum dot, as shown in Fig. 1(a). Accordingly, the all-graphene DB-RTD can also be referred to as a single-quantum-dot RTD.

In this paper a new class of RTDs is proposed based on the concept of cascading two planar graphene quantum dots within a single device, as shown schematically in Fig. 1(b) and (c), which gives rise to a planar all-graphene double-quantum-dot RTD with unique current-voltage characteristics. The transport properties of this proposed device are studied using Nonequilibrium Green's Function (NEGF) formalism and the Extended Huckel (EH) method. The presented results show that the coupling of two quantum dots together, within the same nanoribbon, allows the flow of current at specific bias voltages, only when both dots couple coherently, preventing the flow of current at all other voltages. This gives rise to a giant NDR effect that takes the shape of a current-voltage (I-V) waveform consisting of a single pronounced current peak.

An important measure of NDR is the peak-to-valley current ratio (PVCR), which needs to be maximized. The presented quantum simulation results show that the proposed devices exhibit extremely high PVCR of 50,000, greatly outperforming both experimental reports and theoretical predictions for solid-state [10]–[21] and molecular electronic devices [22]–[27].

Furthermore, it is also shown that due to the planar architecture of the proposed devices, the voltage at which the current peak appears can be tuned by appropriately choosing the dimensions of the quantum dots. Due to the presence of quantized energy states within the quantum dots, the position of the current peak is restricted to specific discrete voltage levels, which enables digitized tunability of its position. By exploiting this property, a multi-peak NDR effect device is presented, using an in-plane parallel connection of multiple tuned devices without the need for any extra fabrication steps.

The presented findings suggest that the proposed devices have unique properties that may facilitate new important electronic devices and components. In the next section of the paper, the calculation method is described, while in the sections that follow, Sections III–VIII, the simulation results are presented and discussed. Section III begins by comparing the transport properties of all-graphene planar double-quantum-dot RTDs with all-graphene planar DB-RTDs, which are referred to in subsequent text as single-quantum-dot RTDs. Then the effect of tuning the dimensions of the quantum dots on the device's I-V characteristics is studied in Section IV, showing how they can be used in order to achieve a multi-peak NDR effect device in Section V. Effect of quantum dot separation, fabrication feasibility and the effect of edge defects are investigated and discussed in Sections VI–VIII respectively. Finally, a conclusion is presented in Section IX.

II. CALCULATION METHOD

Transport calculations for obtaining transmission spectrum plots and I-V characteristic curves were all based on the Extended Huckel (EH) [28] method and Non-Equilibrium Green's Function (NEGF) formalism [29] as implemented in Atomistix Tool Kit (ATK) software package [30].

The device geometries were first optimized and their coordinates were relaxed using the *Tersof* potential [31] until the forces on individual atoms were smaller than 0.001 eV/Å^2. Each device structure was partitioned into three regions: semi-infinite left electrode (L), central scattering region (C), and semi-infinite right electrode (R). The mesh points in real space calculation were defined as uniformly spaced k points of $1 \times 20 \times 50$, with 50 sample points along the transport direction, and 20 along the width.

In the tight-binding model used the tight-binding Hamiltonian was parameterized using a two-center approximation where the matrix elements were described in terms of the overlap between Slater orbitals at each site. The weighting scheme for the orbital energies of the offsite Hamiltonian was according to Wolfsburg and Helmholz [32]. Further details on the calculation method can be found in the ATK manual, in the Semi-Empirical (ATK-SE) package description [33].

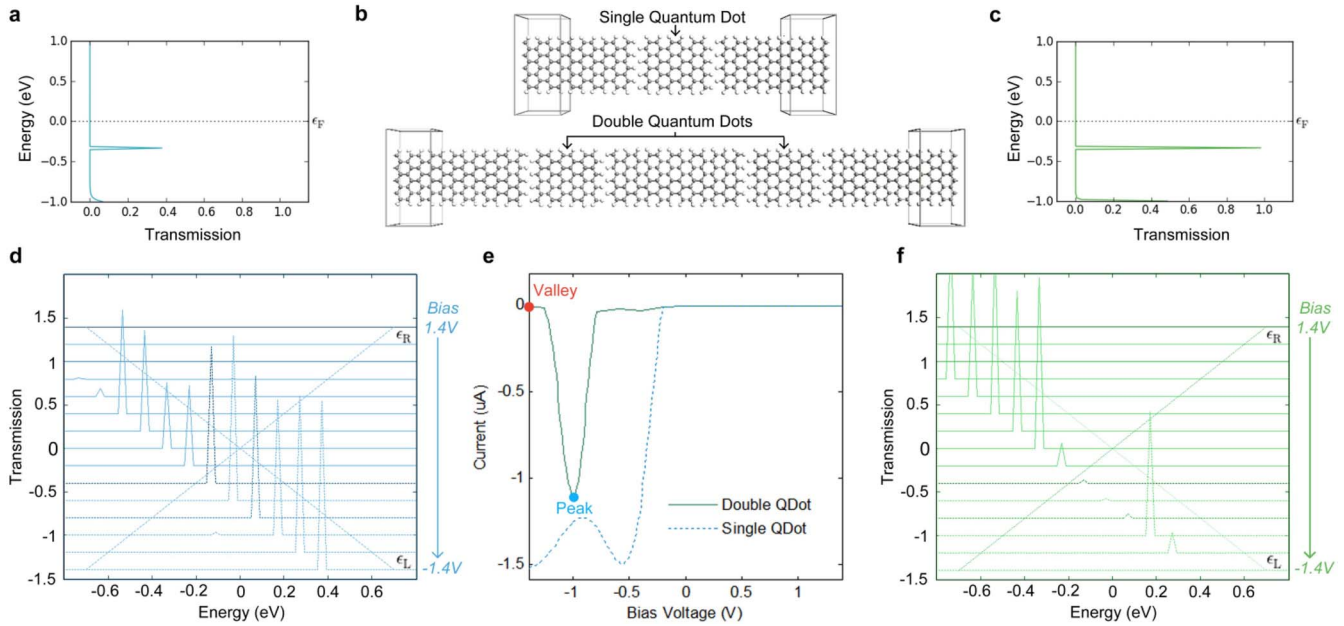

FIGURE 2. Comparison of the transport properties of all-graphene planar single-quantum-dot and double-quantum-dot RTDs. (a) Plots of energy vs. transmission probability at zero bias for the single-quantum-dot RTD, and (c) the double-quantum-dot RTD. (b) Structures of the simulated all-graphene planar single-quantum-dot and double-quantum-dot RTDs. (d) Spectrum of transmission probability vs. energy plots obtained at different bias voltages for the single-quantum-dot RTD and (f) double-quantum-dot RTD. The bias voltage range extends from -1.4 V to 1.4 V, with the lowest plot for a bias of -1.4 V and the highest for a bias of 1.4 V, with increasing 0.2 V steps in between. The region between the Fermi level of the left electrode (ϵ_L) and that of the right electrode (ϵ_R), which are illustrated by the diagonal dotted lines, represents the bias window. (e) Current-voltage characteristics of the single-quantum-dot RTD –dotted blue line– and the double-quantum-dot RTD –solid green line– plotted on the same axes. Peak and valley current points for the double-quantum-dot RTD are marked with blue and red dots respectively.

The electronic transport properties were calculated using NEGF. Coherent transport of electrons was assumed to occur between the electrodes (L) and (R), with Fermi levels μ_L and μ_R, through (C) according to Landauer's formula [34]. The coherent current is equal to:

$$I(V) = \frac{2e}{h}\int_{\mu_R}^{\mu_L} T(E,V)\left[f_0(E-\mu_L) - f_0(E-\mu_R)\right]dE \quad (1)$$

where $T(E,V)$ is the transmission probability of incident electrons with energy E from (L) to (R), $f_0(E-\mu_{L(R)})$ is the Fermi-Dirac distribution function of electrons in (L) and (R) respectively, and $V = (\mu_R - \mu_L)/e$ is the potential difference between (L) and (R). The $T(E,V)$ is correlated with $\hat{G}^a(E)$ and $\hat{G}^r(E)$, the Green's function matrices reflected from (L) and (R) to (C) respectively, as:

$$T(E,V) = Tr\left[\mathrm{Im}\sum_L\left(E-\frac{eV}{2}\right)\hat{G}^r(E)\,\mathrm{Im}\sum_R\left(E+\frac{eV}{2}\right)\hat{G}^a(E)\right] (2)$$

where $\sum_{L(R)}$ are the electrodes' self-energies describing coupling with (C). This same method has been used in previous work [15], [20], [35].

III. TRANSPORT PROPERTIES

In this section the transport properties of a planar all-graphene double-quantum-dot (Double QDot) RTD are studied and compared with those of a planar all-graphene single-quantum-dot (Single QDot) RTD. Both simulated device structures are shown schematically in Fig. 2(b). The overall transport properties of both devices are summarized in Fig. 2.

In the single-quantum-dot RTD, the barriers allow the tunneling of electrons within a narrow energy range only, whilst blocking them at all other energies, as shown in Fig. 2(a), which illustrates the transmission probability of electrons at different energy levels for the single-quantum-dot RTD under zero bias. The figure shows that the transmission probability of electrons at all energies is almost zero, except within a narrow energy window within which resonance occurs, giving rise to the single resonance peak at 0.33 eV below the Fermi level (ϵ_F) of the device. At this energy level of -0.33 eV, the probability of electron transmission across the whole device reaches almost 0.4. On the other hand, for the double-quantum-dot RTD, the presence of the second quantum dot within the same nanoribbon allows coherent coupling with the first quantum dot, facilitating stronger tunneling across the nanoribbon, and making the device almost completely transparent to the transmission of electrons at the resonance peak at which the transmission probability reaches a much higher value of 0.98, as shown in Fig. 2(c). Since the two quantum dots are identical, they would coherently resonate at the same energy level, and since both dots are integrated in a single device within a single nanoribbon, they would coherently couple at the resonance peak, giving rise to an enhanced probability of electron transmission. However, this would also imply that if the two quantum dots had a mismatch in geometry, their coherent coupling

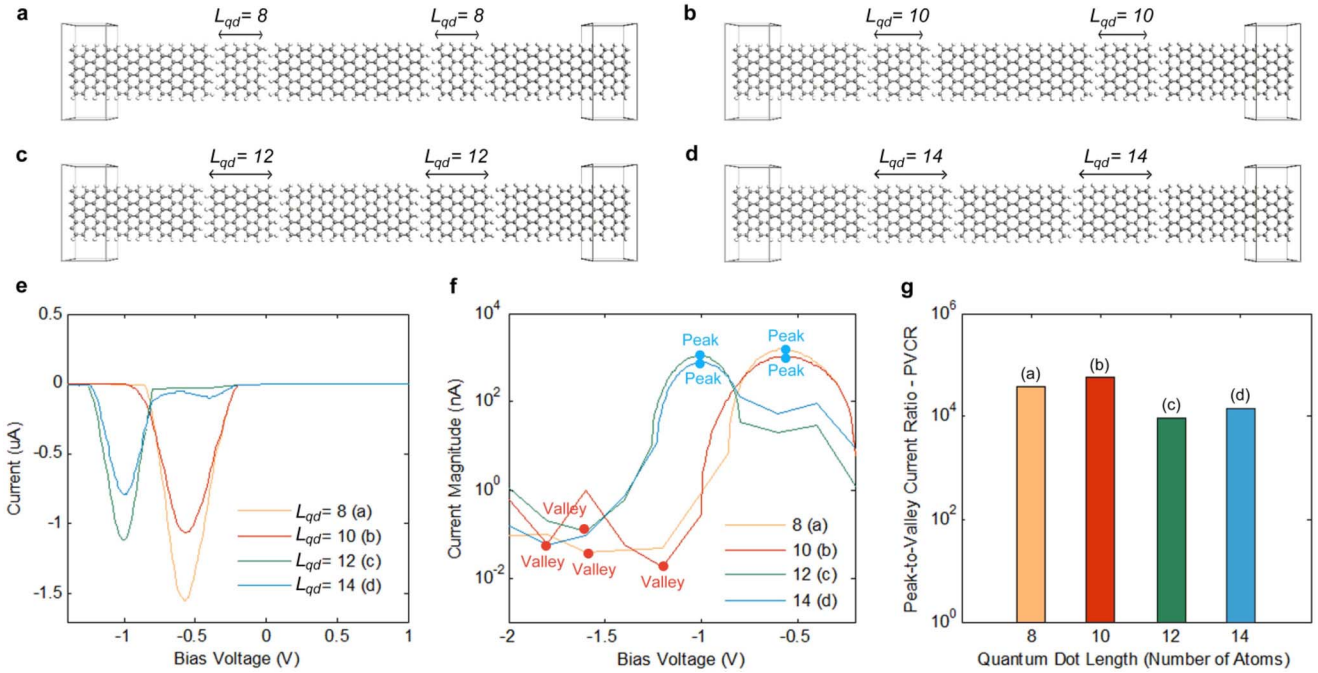

FIGURE 3. Giant tunable NDR effect in planar all-graphene double-quantum-dot RTDs. Four device geometries are shown with equal nanoribbon width and length, but with varying quantum dot lengths of (a) 8, (b) 10, (c) 12 and (d) 14 atoms. The I-V characteristics for the four devices are shown in (e), while a zoom-in at their reverse bias I-V characteristics is shown in (f) with the current axis plotted in log-scale in order to highlight the very low valley current points for all devices. Peak and valley current points are marked with blue and red dots respectively. Achieved PVCR values for the four devices are shown through the bar chart in (g), confirming a consistently high PVCR that exceeds 10^4 in all devices.

might be affected, and this will be investigated later on in Section VIII.

In order for current to flow through the devices, a bias voltage needs to be applied to each of the two devices. In order to investigate the effect of bias voltage on the transport properties of the devices, the transmission spectra of both devices were calculated for a range of bias voltages, and the results are summarized in Fig. 2(d) and (f) for the single-quantum-dot RTD and the double-quantum-dot RTD respectively.

As Fig. 2(d) suggests, for the single-quantum-dot RTD, the bias window either extends above the Fermi level and away from the transmission peak resulting in no current flow under forward bias, or extends below the Fermi level capturing the transmission peak and allowing the flow of current through the device under reverse bias. This effect results in rectification, as shown in Fig. 2(e).

On the other hand, for the double-quantum-dot RTD, as suggested by Fig. 2(f), the transmission peak also lies outside the bias window under forward bias, resulting in no current flow through the device, similar to the single-quantum-dot RTD case. However, under reverse bias the effect of the second quantum dot appears and an interesting phenomenon manifests itself. The transmission peak disappears for most negative bias voltages and only appears within a narrow bias voltage range. This indicates that when the two quantum dots resonate, they result in destructive interference that causes the transmission peak to disappear. Coherent coupling between the two quantum dots only occurs within a narrow voltage range, giving rise to the enhanced transmission peak seen in the transmission spectrum for a bias voltage of -1.0 V, as shown in Fig. 2(f).

The coupling effect of the double-quantum-dots results in a very unique I-V curve that comprises a single pronounced current peak with a giant NDR effect, as shown in Fig. 2(e). This current peak (marked with a blue dot on the figure) reaches a very high value above the 1 μA point. A high current peak in the μA range, is uncommon in tunnelling devices, and is highly favourable, especially for a nanoscale RTD, as it enhances the amount of power that the device is capable of delivering to a connected load.

Past the peak point, current begins to decrease continuously until it reaches the valley point (marked with a red dot on the figure) at which the current magnitude reaches below 1 nA (quantified later on in Fig. 3(f)), representing an extremely high peak-to-valley current ratio (PVCR) in excess of 1000.

IV. CURRENT PEAK TUNABILITY

In this section the effect of varying the quantum dot length within the double-quantum-dot RTD structure is investigated by constructing 4 different double-quantum-dot RTD geometries. The four geometries are shown schematically in Fig. 3(a)–(d) and are constructed from identical nanoribbons that have equal widths and lengths. The difference

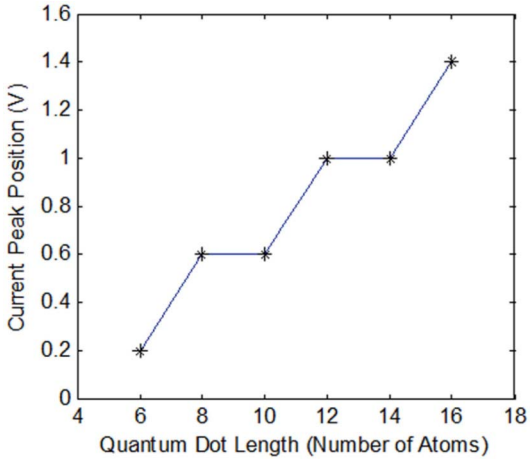

FIGURE 4. Digitized tunability of the current peak position using quantum dot length variation. The figure maps the current peak position in volts to the length of the quantum dots in number of atoms. By varying the length of the quantum dots the current peak position can be tuned across a wide voltage range between discrete voltage levels. All voltage levels are reverse bias voltages, and hence a position of 1.0 V corresponds to a bias of -1.0 V.

between the four geometries is the length of the quantum dots, being 8, 10, 12 and 14 carbon atoms long for the devices of Fig. 3(a)–(d) respectively. The overall length of all devices was kept constant.

The current-voltage (I-V) characteristics of the four devices are shown in Fig. 3(e). Interestingly, the single current peak waveform is achieved consistently for all the four device geometries, confirming its reproducibility.

More interestingly, the plot of Fig. 3(f), with current plotted in logarithmic scale, illustrates that the achieved peak-to-valley current ratio for the four devices is extremely high at values that consistently exceed four orders of magnitude. The valley current levels reach values down to tens of pico-amps, a feature that would be highly desirable for ultra-low power operation in logic and memory devices. Fig. 3(g) summarizes the achieved PVCR for the 4 devices and suggests that not only do they all achieve PVCR values above 10^4 but also, as with the device of Fig. 3(b), can reach values close to 10^5 (50,000 in this case).

A very important observation is noted from Fig. 3(e) regarding the position of the current peak. The device of Fig. 3(a), with a quantum dot length of 8 atoms, has the current peak centered at -0.6 V. Increasing the length of the quantum dots to 10 atoms, as in the device of Fig. 3(b), does not affect the position of the current peak, keeping it centered at -0.6 V. However, a further increase in the length up to 12 atoms, results in a shift in the position of the current peak towards higher voltages, making it centered around -1.0 V. In contrast, another further increase in the length of the quantum dots to 14 atoms does not result in another shift, maintaining the center of the peak at -1.0 V once again. This suggests that a trend is emerging which is investigated by studying more devices with L_{qd} ranging from 6 atoms to 16 atoms, and the results are summarized through the plot of Fig. 4, which maps the current peak position to the length of the quantum dots in atoms. The resulting curve takes a staircase-like shape that indicates the presence of highly quantized energy states within the quantum dots.

The quantized energy states within the quantum dots limit the shifting of the position of the current peak from and to specific discrete voltage levels. In the next subsection this interesting behavior is exploited in achieving an exciting property; multi-peak NDR. However, it is worth pointing out here that this behavior has interesting implications on the fabrication of such devices, as it allows tolerance to fabrication errors, in the range of atoms ($\pm$ 1 atom), that arise when defining the quantum dots within the GNRs. The fabrication method is discussed in more details in the fabrication feasibility section later on.

Careful inspection of Fig. 4 leads to the observation that increasing the quantum dot length results in a shift of the current peak position only at quantum-dot lengths that are multiples of 4 atoms, which correspond to multiples of an armchair graphene nanoribbon unit cell (4 atoms in length). This indicates that only when a complete unit cell is added, the current peak position shifts to a higher voltage, however, when only part of a unit cell is added, the peak's position remains unchanged.

V. MULTI-PEAK NDR EFFECT

While the shifting trend of the current peak can provide interesting insights into the quantum behavior of the devices, the fact that it can be shifted between discrete voltage levels allows digitized tunability, giving rise to a tunable NDR effect. This digitized tunability property, coupled with the planar architecture of the devices, indicates a very interesting device capability that is not possible with field effect devices and very difficult to achieve with vertical tunneling devices; multi-peak NDR [9], [17], [22], [26].

Multi-peak NDR enables exciting device functionalities such as multi-state logic and memory [9], [36] as well as very high frequency multiplication and oscillation [10]–[12]. Multi-peak NDR is hard to achieve in vertical tunneling devices due to the associated complexity in fabrication and results in low PVCR values. However, using the proposed planar double-quantum-dot RTDs a multi-peak NDR effect can be achieved by connecting two double-quantum-dot RTDs in parallel through an in-plane parallel connection, facilitated by their planar architectures, as shown schematically in Fig. 5(a) and (b). One device is tuned to exhibit a current peak at a certain voltage position (-0.6V), while the other is tuned to exhibit the current peak at a different voltage position (-1.0V).

The I-V characteristics of the overall device are shown in Fig. 5(c), and exhibit two pronounced NDR peaks that are clearly distinguishable. In principle this concept can be applied to a larger number of devices in order to achieve a larger number of multiple peaks, without introducing any extra fabrication steps.

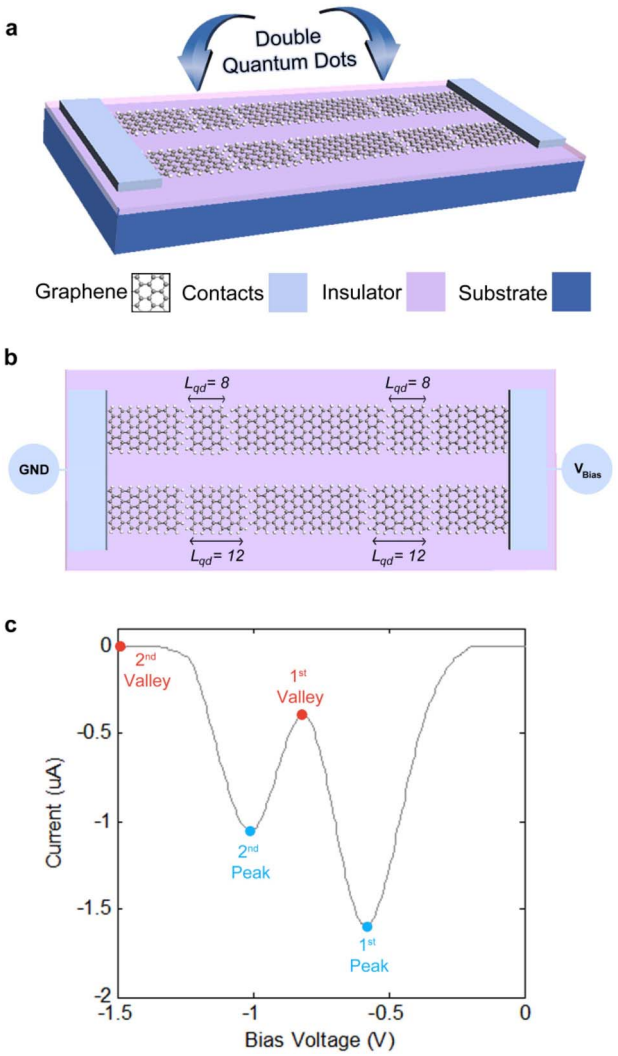

FIGURE 5. **Multi-peak NDR effect in parallel planar all-graphene double-quantum-dot RTDs. (a) Perspective view and (b) top view of two double-quantum-dot RTDs connected in parallel through an in-plane parallel connection. The two devices have different quantum dot lengths (8 and 12 carbon atoms) resulting in different current peak positions and, when connected in parallel, achieve a multi-peak NDR effect, with two pronounced NDR peaks and high peak current values in the micro-amps range, as shown through the device's current-voltage characteristics in (c). Peak and valley current points are marked with blue and red dots respectively.**

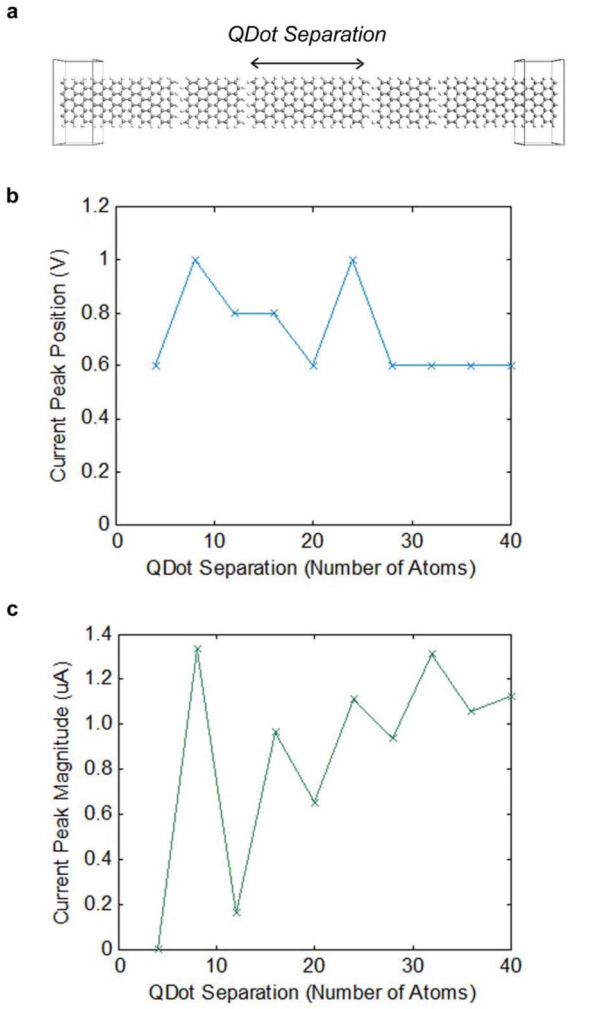

FIGURE 6. **Effect of quantum dot separation on the device's performance. (a) Schematic diagram showing how the length of the graphene nanoribbon between the two quantum dots is used to represent the quantum dot separation distance in atoms. (b) Plot of the variation of the current peak position, between discrete voltage levels, with quantum dot separation distance. All voltage levels are reverse bias voltages, and hence a current peak position of 1.0 V corresponds to a bias of -1.0 V. (c) Plot of the variation of the current peak's magnitude with quantum dot separation distance.**

VI. QUANTUM DOT SEPARATION

In this section we investigate the effect of varying the separation distance between the two quantum dots on the device's performance, by varying the length of the graphene nanoribbon between them as shown in Fig. 6(a).

The length of the graphene nanoribbon that connects the two quantum dots in the device shown in Fig. 6(a) was varied from a single unit cell (4 atoms in length) to 10 unit cells (40 atoms in length), in increments of single unit cells, and the corresponding I-V characteristics were calculated for each device configuration. In all device configurations the single-current-peak I-V waveform was observed, however, the current peak's position and its magnitude varied with the variation of the quantum dot separation distance. Fig. 6(b) and (c) plot the variation of the current peak position and the variation of the current peak magnitude, with quantum dot separation distance, respectively.

The current peak's position, plotted in Fig. 6(b), is the reverse bias voltage at which the current peak appears, and hence a current peak position of 1.0 V would correspond to a bias of -1.0 V. Fig. 6(b) suggests that when the two quantum dots are close to each other, they interact and interfere resulting in an unstable current peak position that is highly affected by the separation distance. However, as the distance is increased beyond 25 atoms, the current peak's position stabilizes at a reverse bias voltage of 0.6 V. A similar trend is also observed in Fig. 6(c), in which the current peak's magnitude shows great variation at small separation distances,

but begins to stabilize as the separation distance is increased. It is also noted, that at the minimal separation distance of a single unit cell (4 atoms) the current peak's magnitude is drastically suppressed to a very low value close to zero, suggesting that when the two quantum dots are brought in close proximity they destructively interfere resulting in the observed demolition of the current peak's magnitude.

VII. FABRICATION FEASIBILITY

The proposed devices are planar devices that do not require any external gating, doping or stacking of material layers. Their fabrication can be achieved by the following steps. Once a Graphene monolayer is transferred to an insulating substrate, it can be patterned into the device structure using a single photo-lithography step. Metallic contacts such as platinum or gold, as shown in Figs. 1 and 5, are then formed. It is important to note that this process gives rise to GNRs with rough edges [37], and may not be able to define narrow trenches for the tunnel barriers. Before volume fabrication, the performance of such devices would require a Monte Carlo simulation study, in order to investigate the effect of GNR edge roughness on the device's performance, specifically its resonant behavior. However, an investigation of the effect of the presence of edge defects, rather than random edge roughness, within the device is possible using quantum simulations. Such a study can provide insights about where would the presence of defects be most critical to the device's performance, and this will be presented in Section VIII.

Nevertheless, the experimental realization of small production volumes of the devices proposed here may be achieved by first realizing GNRs with smooth edges, and then precisely etching the insulating trenches within them using high precision etching techniques.

The experimental realization of GNRs with smooth edges has proven to be a challenge, however, recent work has shown promising results towards achieving this goal [38]–[44], and a number of experimental reports have reported techniques to achieve this [40]–[42]. As for the precise etching of the insulating trenches, this may be performed using Helium Ion Beam lithography [45]–[47] or single-atom catalyst chiseling [43], both of which have been able to achieve high resolution patterning of Graphene.

Any remaining fabrication errors that arise as a result of using such high resolution methods are expected to be in the order of atoms, and such small errors are expected to be tolerable in the proposed devices due to the reproducibility of their NDR effect with varying quantum dot lengths, as was suggested earlier through Fig. 3, and due to the fact that the position of the current peak in them does not shift if the length of the quantum dot is fabricated an atom or two more than what it was designed for, as was suggested earlier through Fig. 4. Nevertheless, further experimental efforts are a very important step towards consolidating these very interesting physical insights.

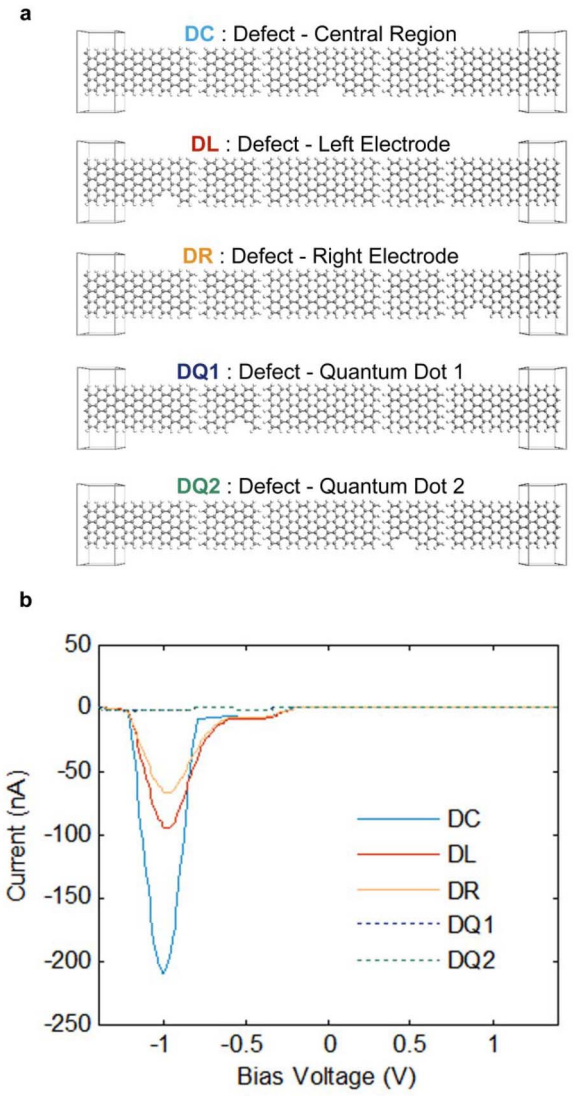

FIGURE 7. Effect of edge defects on device performance. (a) Five different double QDot RTD device configurations with edge defects introduced at five different positions; the central region (DC), the left electrode (DL), the right electrode (DR), the first quantum dot (DQ1) and the second quantum dot (DQ2). (b) I-V characteristics of the device configurations shown in (a).

VIII. EFFECT OF EDGE DEFECTS

This section presents a preliminary study of the effect of the presence of edge defects on the device's performance. The effect of edge defects located at different positions along the double QDot RTD device structure, shown in Fig. 2(b) earlier, was investigated. The defects were introduced at five different positions giving rise to five different device configurations: a device with a defect in the central region (DC), the left electrode (DL), the right electrode (DR), the first quantum dot (DQ1) and the second quantum dot (DQ2), and these are shown schematically in Fig. 7(a), top to bottom, respectively.

The corresponding I-V characteristics of the five device configurations are shown in Fig. 7(b). It can be seen through the figure that devices with defects outside the

quantum dots (DC, DL and DR) continue to exhibit the single-current-peak I-V characteristics maintaining the current peak at its position and showing strong NDR behavior. The presence of the defect seems to have a damping effect on the current peak, resulting in a slightly suppressed current peak magnitude when compared to the device with no defects [Fig. 2(e)]. This suppression is stronger for the defects in the left and right electrodes than it is for the defect within the central region.

On the other hand, device configurations with defects inside the quantum dots (DQ1 and DQ2) do not exhibit a current peak and do not show any significant current flow, suggesting that the presence of edge defects within the quantum dots is most critical and can be very detrimental for the operation of the double QDot RTD. This might be due to the fact that a defect in one of the quantum dots creates a mismatch between it and the other quantum dot, and hence prevents it from coherently coupling with it at the resonance peak. The loss of coherent coupling will result in the blockage of electron flow by the defected quantum dot at the resonance peak and hence the prevention of current flow through the device, as was observed in Fig. 7(b). These results indicate that the quantum dots need careful attention during fabrication, while defects outside of the quantum dots may not be as detrimental.

IX. CONCLUSION

In summary, a new class of planar NDR devices was presented, termed as all-graphene planar double-quantum-dot RTDs, which can be realized completely within single graphene nanoribbons. Quantum simulation results have shown that such devices exhibit a very interesting property of having a single pronounced current peak in their I-V characteristics, resulting in a giant NDR effect that exhibits PVCR values exceeding four orders of magnitude. Such a property takes place due to destructive interference between the cascaded quantum dots, which only couple coherently within a narrow bias voltage range, under which current conduction occurs. By tuning the dimensions of the quantum dots the voltage at which this coherent coupling occurs can be tuned, allowing tunability of the current peak position. Due to the presence of quantized energy states within the quantum dots, the current peak position can only be tuned between discrete voltage levels, enabling digitized tunability. It was shown how this property can be exploited in order to achieve a multi-peak NDR effect device through an in-plane parallel connection of multiple tuned devices. The findings presented here suggest a promising potential for the application of planar double-quantum-dot RTDs in next generation electronics.

ACKNOWLEDGMENT

Authors would like to thank the optics & nanoelectronics research group members for valuable discussions

REFERENCES

[1] K. S. Novoselov *et al.*, "A roadmap for graphene," *Nature*, vol. 490, pp. 192–200, Oct. 2012.

[2] A. K. Geim, "Graphene: Status and prospects," *Science*, vol. 324, pp. 1530–1534, Jun. 2009.

[3] P. Avouris, "Graphene: Electronic and photonic properties and devices," *Nano Lett.*, vol. 10, pp. 4285–4294, Sep. 2010.

[4] L. Britnell *et al.*, "Field-effect tunneling transistor based on vertical graphene heterostructures," *Science*, vol. 335, pp. 947–950, Feb. 2012.

[5] C. O. Kim *et al.*, "High photoresponsivity in an all-graphene p–n vertical junction photodetector," *Nat. Commun.*, vol. 5, Feb. 2014, Art. ID 3249.

[6] S. Kim *et al.*, "Graphene p–n vertical tunneling diodes," *ACS Nano*, vol. 7, pp. 5168–5174, Jun. 2013.

[7] A. M. Ionescu and H. Riel, "Tunnel field-effect transistors as energy-efficient electronic switches," *Nature*, vol. 479, pp. 329–337, Nov. 2011.

[8] L. Esaki, "New phenomenon in narrow germanium p–n junctions," *Phys. Rev.*, vol. 109, pp. 603–604, Jan. 1958.

[9] P. Mazumder, S. Kulkarni, M. Bhattacharya, J. P. Sun, and G. I. Haddad, "Digital circuit applications of resonant tunneling devices," *Proc. IEEE*, vol. 86, no. 4, pp. 664–686, Apr. 1998.

[10] E. R. Brown *et al.*, "Oscillations up to 712 GHz in InAs/AlSb resonant−tunneling diodes," *Appl. Phys. Lett.*, vol. 58, pp. 2291–2293, May 1991.

[11] T. C. L. G. Sollner, W. D. Goodhue, P. E. Tannenwald, C. D. Parker, and D. D. Peck, "Resonant tunneling through quantum wells at frequencies up to 2.5 THz," *Appl. Phys. Lett.*, vol. 43, pp. 588–590, Jul. 1983.

[12] S. Suzuki, M. Asada, A. Teranishi, H. Sugiyama, and H. Yokoyama, "Fundamental oscillation of resonant tunneling diodes above 1 THz at room temperature," *Appl. Phys. Lett.*, vol. 97, Dec. 2010, Art. ID 242102.

[13] A. Mishchenko *et al.*, "Twist-controlled resonant tunnelling in graphene/boron nitride/graphene heterostructures," *Nat. Nanotechnol.*, vol. 9, pp. 808–813, Sep. 2014.

[14] R. Tsu and L. Esaki, "Tunneling in a finite superlattice," *Appl. Phys. Lett.*, vol. 22, pp. 562–564, Mar. 1973.

[15] F. Al-Dirini, F. M. Hossain, A. Nirmalathas, and E. Skafidas, "All-graphene planar double barrier resonant tunneling diodes," *IEEE J. Electron Devices Soc.*, vol. 2, no. 5, pp. 118–122, Sep. 2014.

[16] G. Fiori, "Negative differential resistance in mono and bilayer graphene p-n junctions," *IEEE Electron Device Lett.*, vol. 32, no. 10, pp. 1334–1336, Oct. 2011.

[17] H. Inokawa, A. Fujiwara, and Y. Takahashi, "Multipeak negative-differential-resistance device by combining single-electron and metal-oxide-semiconductor transistors," *Appl. Phys. Lett.*, vol. 79, pp. 3618–3620, Sep. 2001.

[18] Y. Song, H.-C. Wu, and Y. Guo, "Negative differential resistances in graphene double barrier resonant tunneling diodes," *Appl. Phys. Lett.*, vol. 102, Mar. 2013, Art. ID 093118.

[19] H. Teong, K.-T. Lam, S. B. Khalid, and G. C. Liang, "Shape effects in graphene nanoribbon resonant tunneling diodes: A computational study," *J. Appl. Phys.*, vol. 105, Apr. 2009, Art. ID 084317.

[20] F. Al-Dirini, F. M. Hossain, A. Nirmalathas, and E. Skafidas, "Asymmetrically-gated graphene self-switching diodes as negative differential resistance devices," *Nanoscale*, vol. 6, pp. 7628–7634, Apr. 2014.

[21] K. Ismail, B. S. Meyerson, and P. J. Wang, "Electron resonant tunneling in Si/SiGe double barrier diodes," *Appl. Phys. Lett.*, vol. 59, pp. 973–975, Aug. 1991.

[22] M. Sadek, M. Wierzbowska, M. F. Rode, and A. L. Sobolewski, "Multipeak negative differential resistance from interplay between nonlinear stark effect and double-branch current flow," *RSC Adv.*, vol. 4, pp. 52933–52939, Oct. 2014.

[23] J. Zhou, S. Samanta, C. Guo, J. Locklin, and B. Xu, "Measurements of contact specific low-bias negative differential resistance of single metalorganic molecular junctions," *Nanoscale*, vol. 5, pp. 5715–5719, May 2013.

[24] J. Chen, M. A. Reed, A. M. Rawlett, and J. M. Tour, "Large on–off ratios and negative differential resistance in a molecular electronic device," *Science*, vol. 286, pp. 1550–1552, Nov. 1999.

[25] I. Kratochvilova *et al.*, "Room temperature negative differential resistance in molecular nanowires," *J. Mater. Chem.*, vol. 12, pp. 2927–2930, Aug. 2002.
[26] E. D. Mentovich *et al.*, "Multipeak negative-differential-resistance molecular device," *Small*, vol. 4, pp. 55–58, Jan. 2008.
[27] M. L. Perrin *et al.*, "Large negative differential conductance in single-molecule break junctions," *Nat. Nanotechnol.*, vol. 9, pp. 830–834, Aug. 2014.
[28] K. Stokbro *et al.*, "Semiempirical model for nanoscale device simulations," *Phys. Rev. B Condens. Mat. Mater. Phys.*, vol. 82, Aug. 2010, Art. ID 075420.
[29] M. Brandbyge, J. L. Mozos, P. Ordejón, J. Taylor, and K. Stokbro, "Density-functional method for nonequilibrium electron transport," *Phys. Rev. B Condens. Mat. Mater. Phys.*, vol. 65, Mar. 2002, Art. ID 1654011.
[30] QuantumWise. (Apr. 9, 2015). *ATK-SE Package (13.8)*. [Online]. Available: http//www.quantumwise.com
[31] J. Tersoff, "New empirical approach for the structure and energy of covalent systems," *Phys. Rev. B*, vol. 37, pp. 6991–7000, Apr. 1988.
[32] M. A. X. Wolfsberg and L. Helmholz, "The spectra and electronic structure of the tetrahedral ions MnO_4-, CrO_4-, and ClO_4-," *J. Chem. Phys.*, vol. 20, pp. 837–843, Jan. 1952.
[33] F. Sols, F. Guinea, and A. Neto, "Coulomb blockade in graphene nanoribbons," *Phys. Rev. Lett.*, vol. 99, Oct. 2007, Art. ID 166803.
[34] R. Landauer, "Spatial variation of currents and fields due to localized scatterers in metallic conduction," *IBM J. Res. Develop.*, vol. 1, pp. 223–231, Jul. 1957.
[35] F. Al-Dirini, F. M. Hossain, A. Nirmalathas, and E. Skafidas, "All-graphene planar self-switching MISFEDs, metal-insulator-semiconductor field-effect diodes," *Sci. Rep.*, vol. 4, Feb. 2014, Art. ID 3983.
[36] R. H. Mathews *et al.*, "A new RTD-FET logic family," *Proc. IEEE*, vol. 87, no. 4, pp. 596–605, Apr. 1999.
[37] M. Y. Han, B. Özyilmaz, Y. Zhang, and P. Kim, "Energy band-gap engineering of graphene nanoribbons," *Phys. Rev. Lett.*, vol. 98, May 2007, Art. ID 206805.
[38] J. Cai *et al.*, "Atomically precise bottom-up fabrication of graphene nanoribbons," *Nature*, vol. 466, pp. 470–473, Jul. 2010.
[39] L. C. Campos, V. R. Manfrinato, J. D. Sanchez-Yamagishi, J. Kong, and P. Jarillo-Herrero, "Anisotropic etching and nanoribbon formation in single-layer graphene," *Nano Lett.*, vol. 9, pp. 2600–2604, Jun. 2009.
[40] H. Huang *et al.*, "Spatially resolved electronic structures of atomically precise armchair graphene nanoribbons," *Sci. Rep.,* vol. 2, Dec. 2012, Art. ID 983.
[41] K. Kim *et al.*, "Atomically perfect torn graphene edges and their reversible reconstruction," *Nat. Commun.*, vol. 4, Nov. 2013, Art. ID 2723.
[42] C. Tao *et al.*, "Spatially resolving edge states of chiral graphene nanoribbons," *Nat. Phys.*, vol. 7, pp. 616–620, May 2011.
[43] W. L. Wang *et al.*, "Direct observation of a long-lived single-atom catalyst chiseling atomic structures in graphene," *Nano Lett.*, vol. 14, pp. 450–455, Jan. 2014.
[44] X. Wang *et al.*, "Graphene nanoribbons with smooth edges behave as quantum wires," *Nat. Nanotechnol.*, vol. 6, pp. 563–567, Aug. 2011.
[45] A. N. Abbas *et al.*, "Patterning, characterization, and chemical sensing applications of graphene nanoribbon arrays down to 5 nm using helium ion beam lithography," *ACS Nano*, vol. 8, pp. 1538–1546, Jan. 2014.
[46] D. C. Bell, M. C. Lemme, L. A. Stern, J. R. Williams, and C. M. Marcus, "Precision cutting and patterning of graphene with helium ions," *Nanotechnology*, vol. 20, Nov. 2009, Art. ID 455301.
[47] M. C. Lemme *et al.*, "Etching of graphene devices with a helium ion beam," *ACS Nano*, vol. 3, pp. 2674–2676, Sep. 2009.

FERAS AL-DIRINI (S'08) received the B.Sc. degree (Highest Hons.) in electronics engineering from the Princess Sumaya University for Technology, Jordan, in 2011. He has recently submitted his Ph.D. thesis in the Department of Electrical and Electronic Engineering, University of Melbourne, Australia, where he was recently employed, after submission of his Ph.D. thesis, as a Researcher with the Centre for Neural Engineering.

In 2009 and 2010, he was an exchange student with the University of Illinois at Urbana–Champaign, USA, and in the summer of 2009, he was a Research Intern with the Institute for Microsystems Technology, Technical University of Hamburg-Harburg, Germany. His research interests are in the fields of nanoelectronics and nanotechnology, such as graphene devices, nano biosensors, and post-CMOS electronics. He has authored and co-authored about 20 publications in the above fields in leading journals and conferences, including *Nanoscale*, the IEEE JOURNAL OF ELECTRON DEVICES SOCIETY, *Scientific Reports,* and *Applied Physics Letters*.

Mr. Al-Dirini was a recipient of the Australian Postgraduate Award and the National ICT Australia Ph.D. Top-Up Scholarship from 2011 to 2015. He is a member of the Australian Nanotechnology Network.

MAHMOOD A. MOHAMMED received the B.Sc. degree (Highest Hons.) in electronics engineering and the master's degree (Highest Hons.) in electrical engineering from the Princess Sumaya University for Technology (PSUT) in 2011 and 2015, respectively. In 2011, he was an intern with the Ergonomics Research Group, Department of Mechanical Engineering, University of South Australia (UniSA), Adelaide, Australia. His research interests are in the fields of CMOS analog circuits design, very large-scale integration design, and device physics. During the past three years, he has authored and co-authored seven technical refereed journal and conference publications in the field of analog and mixed signal circuits design. He was a Teaching Assistant with the Department of Electrical Engineering, PSUT, for electronics, digital electronics, and communication electronics courses. He received full scholarships, awarded to outstanding students, in order to complete his B.Sc. and M.S.E.E. degrees at PSUT.

FARUQUE M. HOSSAIN was born in Faridpur, Bangladesh, in 1968. He received the M.Sc. degree in applied physics and electronics from the University of Dhaka, Bangladesh, in 1993, the M.Eng.Sc. degree in electrical engineering (majoring in photovoltaics) from the University of New South Wales, Australia, in 2000, and the Ph.D. degree in materials engineering from the Tokyo Institute of Technology, Japan, in 2003.

He has undertaken subsequent post-doctoral fellowships at the University of Newcastle (jointly with the University of New South Wales), and the University of Melbourne in solid state materials science, surface science, photo-catalysis, condensed-matter physics, and quantum physics and chemistry. His current research interests are on the structural, mechanical, electronic, magnetic, and optical properties of graphene and other 2-D nanostructures, thin-films, reactive surfaces and interfaces, to find potential applications in bio-nano-sensors, molecular single-electron transistors, molecular junctions and devices for biocompatible sensors, nano-scale chips, and nanocomputer applications.

Dr. Faruque is a Reviewer of the IEEE TRANSACTIONS ON ELECTRON DEVICES.

THAS (AMPALAVANAPILLAI) NIRMALATHAS (SM'03) received the B.Eng. and Ph.D. degrees in electrical and electronic engineering from the University of Melbourne, in 1993 and 1998, respectively.

He is a Professor of Electrical and Electronic Engineering with the University of Melbourne, Australia. He is also the Director of the Melbourne Networked Society Institute. He also directs the Australia's first university based start-up accelerator—Melbourne Accelerator Program, aimed at promoting entrepreneurship culture on campus. From 2000 to 2004, he was the Director of Photonics Research Laboratory (Melbourne Node of Australian Photonics CRC) and also the Program Leader of Telecommunications Technologies Program. From 2004 to 2006, he was the Program Leader for the Network Technologies Research Program in National ICT Australia (NICTA), a premier Australian research center of excellence in ICT. He was also the acting Lab Director of VRL in 2007. From 2006 to 2008, he was the Research Group Manager of the Networked Systems Group of Victoria Research Laboratory at the NICTA. From 2010 to 2013, he was the Head of the Department of Electrical and Electronic Engineering. He has written over 400 technical articles and currently holds three active international patents. His research interests include microwave photonics, fiber-radio or fiber wireless systems, optical access networks, optical wireless transmission and networks, and optical-wireless network integration.

Prof. Nirmalathas was a Guest Editor for the Special Issue on Opto-Electronics and Communications of the *IEICE Transactions in Communications*. From 2007 to 2013, he has been an Associate Editor of the IEEE/OSA JOURNAL OF LIGHTWAVE TECHNOLOGY. He is currently on the Editorial Panel of the *Photonics and Networks SPIE Journal*. He is a member of Optical Society of America and a fellow of the Institution of Engineers Australia.

EFSTRATIOS SKAFIDAS (M'98–SM'02) received the Ph.D. degree in 1998, and since then he has focused his research in the areas of novel nano-electronic systems, communications technologies, and biosensors. His work has led to innovative new millimeter wave communication systems on CMOS and is the basis on new biomedical devices. He is currently a Professor of Nanoelectronics and the Director of the Centre for Neural Engineering (CfNE), University of Melbourne. He has played an integral role in establishing the CfNE, an interdisciplinary center established to undertake research in neursoscience and neural diseases by drawing together Australia's leading neuroscientists, neurologists, psychiatrists, chemists, physicists, and engineers. His research is currently incorporated in multiple international communication standards and has led to the establishment of two start-up companies.

Prof. Skafidas is a fellow of the Institution of Engineers Australia and the Australian Academy of Technological Sciences and Engineering.